J|A|C|S ARTICLES

Published on Web 11/23/2009

Laterally Azo-Bridged H-Shaped Ferroelectric Dimesogens for Second-Order Nonlinear Optics: Ferroelectricity and Second Harmonic Generation

Yongqiang Zhang,*,† Josu Martinez-Perdiguero,‡ Ute Baumeister,⊥ Christopher Walker,† Jesus Etxebarria,*,‡ Marko Prehm,⊥ Josu Ortega,§ Carsten Tschierske,|| Michael J. O'Callaghan,† Adam Harant,† and Mark Handschy†,#

Displaytech Inc., 2602 Clover Basin Drive, Longmont, Colorado 80503, University of the Basque Country, 48080 Bilbao, Spain, and Institute of Chemistry, MLU Halle-Wittenberg, Kurt-Mothes-Strasse 2, D-06120 Halle, Germany

Received August 14, 2009; E-mail: yqzhang@micron.com; j.etxeba@ehu.es

Abstract: Two classes of laterally azo-bridged H-shaped ferroelectric liquid crystals (FLCs), incorporating azobenzene and disperse red 1 (DR-1) chromophores along the FLC polar axes, were synthesized and characterized by polarized light microscopy, differential scanning calorimetry, 2D X-ray diffraction analysis, and electro-optical investigations. They represent the first H-shaped FLC materials exhibiting the ground-state, thermodynamically stable enantiotropic SmC* phase, i.e., ground-state ferroelectricity. Second harmonic generation measurements of one compound incorporating a DR-1 chromophore at the incident wavelength of 1064 nm give a nonlinear coefficient of $d_{22} = 17$ pm/V, the largest nonlinear optics coefficient reported to date for calamitic FLCs. This value enables viable applications of FLCs in nonlinear optics.

Introduction

Dramatic advances in the study of organic nonlinear optical (NLO) materials, potential successors to inorganic crystals such as $LiNO_3$, have occurred in recent years.[1] Organic materials offer potential advantages over inorganic crystals because of their attractive features such as low dielectric constants, large and ultrafast responses, facile fabrication and processability, and wide range of operating frequencies. In poled-polymer materials, macroscopic nonlinearities are generally achieved by using an extremely strong electric field. Nevertheless, the poled state is not thermodynamically stable, causing electro-optic performance to decay over time. Although it is possible to maintain a stable dipole alignment by utilizing either side-chain polymers with high glass transition temperature (T_g) or cross-linking polymers, it is difficult to realize both large macroscopic nonlinear effects and stable dipole alignment in the same system.[1h]

Ferroelectric liquid crystals (FLCs), as new types of organic NLO materials, possess inherent thermodynamically stable polar order.[2,3] If a large second-order susceptibility ($\chi^{(2)}$) can be incorporated, NLO FLCs will become a compelling alternative to inorganic and poled-polymer materials. An important advantage is that their polar direction can be controlled via ferroelectric (FE) switching under an external electric field, enabling fabrication of more complex devices. Previous attempts to make rod-shaped NLO FLCs have proved the principle,[4] but they have been deficient in the size of their NLO coefficients because incorporating chromophores possessing large *hyperpolarizabilities* (β) along their polar axis while remaining an FLC is extremely difficult.[5] A new approach to making complex FLCs with potentially large NLO coefficients was pioneered by the Walba group,[6] based on a novel "H-shaped" molecular structure including disperse red 1 (DR-1), in which a pair of rod-shaped molecules are connected by an azo bridge. Note that the structural array has two important advantages: (i) a wider range of chromophores can be accommodated, and (ii) it more fully aligns the chromophore along the FLC's polar axis, thereby producing larger electro-optical coefficients. Although few such

† Displaytech Inc. (Displaytech Inc. is now part of Micron Technology Inc.).
‡ Department of Condensed Matter Physics, University of the Basque Country.
§ Applied Physics II, University of the Basque Country.
⊥ Physical Chemistry, MLU Halle-Wittenberg.
|| Organic Chemistry, MLU Halle-Wittenberg.
Present address: Office of the Under Secretary, Department of Energy, 1000 Independence SW, Washington, DC 20585.

(1) (a) Lee, M.; Katz, H. E.; Erben, C.; Gill, D. M.; Gopalan, P.; Heber, J. D.; McGee, J. *Science* **2002**, *298*, 1401. (b) Shi, Y.; Zhang, C.; Zhang, H.; Bechtel, J. H.; Dalton, L. R.; Robinson, B. H.; Steier, W. H. *Science* **2000**, *288*, 119. (c) *Nonlinear optics of organic molecules and polymers*; Nalwa, H. S., Miyata, S., Eds.; CRC Press, Inc: Boca Raton, FL, 1996. (d) Cole, J. M. *Philos. Trans. R. Soc. London A* **2003**, *361*, 2751. (e) Huang, D.; Parker, T.; Guan, H. W.; Cong, S.; Jin, D.; Dinu, R.; Chen, B.; Tolstedt, D.; Wolf, N.; Condon, S. *SPIE* **2005**, *5624*, 172. (f) Marder, S. R. *Chem. Commun.* **2006**, 131. (g) Innocenzi, P.; Lebeau, B. *J. Mater. Chem.* **2005**, *15*, 3821. (h) Ma, H.; Chen, B.; Sassa, T.; Dalton, L. R.; Jen, A. K.-Y. *J. Am. Chem. Soc.* **2001**, *123*, 986. (i) Coe, B. J. *Acc. Chem. Res.* **2006**, *39*, 383.

(2) Lagerwall, S. T. *Ferroelectric and antiferroelectric liquid crystals*; Wiley-VCH: Weinheim, Germany, 1999.

(3) Although polymeric nematic liquid crystals have been shown to possess permanent polar order and strong SHG activity, they cannot respond to the applied electric field as well as FLCs owing to the high viscosity of polymers: (a) Watanabe, T.; Miyata, S.; Furakawa, T.; Takezoe, H.; Nishi, T.; Migita, A.; Sone, M.; Watanabe, J. *Jpn. J. Appl. Phys.* **1996**, *35*, L505. (b) Koike, M.; Yen, C.-C.; Liu, Y.; Tsuchiya, H.; Tokita, M.; Kawauchi, S.; Takezoe, H.; Watanabe, J. *Macromolecules* **2007**, *40*, 2524–2531.

 10.1021/ja9069166

Chart 1. H-Shaped FLC Compounds (Chromophores in Blue)

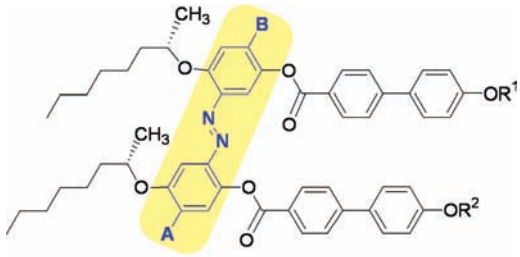

1a: A = B = H, $R^1 = R^2 = C_{10}H_{21}$
1b: A = B = H, $R^1 = R^2 = C_8H_{16}$ C_5H_{11} (linolyl)
1c: A = B = H, $R^1 = R^2 = C_{11}H_{22}SiMe_2CH_2SiMe_3$
1d: A = B = H, $R^1 = R^2 = C_{11}H_{22}SiMe_3$
1e: A = B = H, $R^1 = R^2 = C_9H_{18}CH{=}CH_2$

2a: A = NEt_2, B = NO_2, $R^1 = R^2 = C_{10}H_{21}$
2b: A = NEt_2, B = NO_2, $R^1 = R^2 = C_9H_{18}CH{=}CH_2$
2c: A = NEt_2, B = NO_2, $R^1 = C_{10}H_{21}$, $R^2 = C_9H_{18}CH{=}CH_2$

compounds have been reported,[6] none, with the exception of a main-chain polymer[6b] derived from one of these compounds, exhibits the desired thermodynamically stable enantiotropic SmC*, i.e., ferroelectric, phase which is indispensable to applications of FLCs in nonlinear optics.

Herein, we first report two classes of laterally azo-bridged H-shaped FLCs, **1a**−**e** and **2a**−**c** (Chart 1), that exhibit a ground-state, thermodynamically stable enantiotropic SmC* phase, i.e., ground-state ferroelectricity. Compounds **1a**−**e** include a conjugated azo linkage, while **2a**−**c** are incorporated into a DR-1 chromophore. Second harmonic generation (SHG) measurements show that the extrapolated d_{22} coefficient of the second-order susceptibility tensor for **2c** is 17 pm/V, *the largest NLO coefficient reported to date for calamitic NLO FLCs*. It should be noted that chromophores in these materials can be readily oriented by a weak electric field (0.1−0.5 V μm^{-1}) parallel to the cell surface of a homeotropically aligned cell. In contrast, the poling process for poled polymers generally requires a much stronger electric field (10−50 V μm^{-1}) at high temperature (above the polymer glass-transition temperature, T_g), which requires NLO chromophores to possess excellent thermal and chemical stability.[1c,7]

Scheme 1. Synthesis of H-Shaped FLC Compounds **1a**−**e** Incorporating an Azobenzene Chromophore[a]

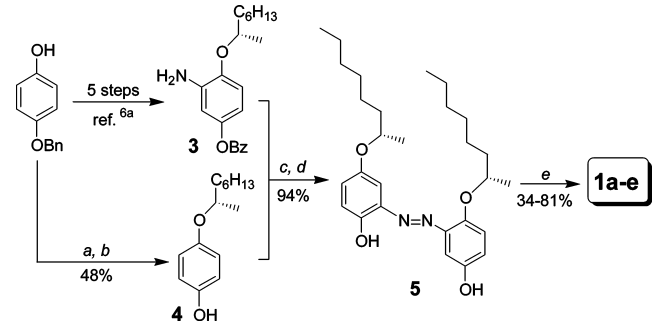

[a] Reagents and conditions: (a) (−)-R-2-octanol, PPh_3, DEAD, THF. (b) $Pd(OH)_2/C$, H_2. (c) **3**, HCl, $NaNO_2$; then **4**, K_2CO_3, H_2O/EtOH.[8] (d) $BuNH_2$, benzene.[9] (e) 4′-Alkoxy-4-biphenylcarboxylic acid chlorides, DMAP, Et_3N, THF. Bn = benzyl, Bz = benzoyl.

Scheme 2. Synthesis of H-Shaped FLC Compounds **2a**−**c** Incorporating a DR-1 Chromophore[a]

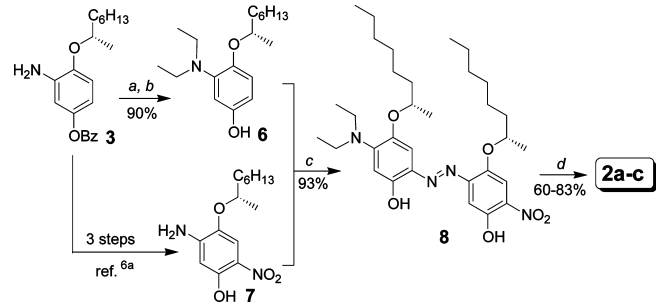

[a] Reagents and conditions: (a) CH_3CHO, $Na(AcO)_3BH$, $ClCH_2CH_2Cl$.[10] (b) LiOH, EtOH, H_2O. (c) **7**, HCl, $NaNO_2$, EtOH/H_2O; then **6**, pyridine, CH_2Cl_2, EtOH. (d) 4′-Alkoxy-4-biphenylcarboxylic acid chlorides, DMAP, Et_3N, THF.

Results and Discussion

Synthesis. The syntheses of two types of compounds, **1a**−**e** and **2a**−**c**, are outlined in Schemes 1 and 2, respectively (see detailed synthetic procedures and analytic data in the Supporting Information). To prepare compounds **1**, two precursors for diazo coupling reactions, **3** and **4**, were synthesized from 4-benzyloxyphenol by a literature[6a] approach (for **3**) and a two-step approach (for **4**) involving Mitsunobu reaction and benzyl deprotection via hydrogenolysis. Subsequent diazo coupling,[8] followed by aminolysis of the resulted ester under mild conditions,[9] afforded diphenol **5** in excellent yield. Esterification of **5** with a variety of 4′-alkoxy-4-biphenylcarboxylic acid chlorides generated the final mesogens **1a**−**e** in moderate to good yields (Scheme 1). As shown in Scheme 2, the final mesogens **2a**−**c** were synthesized from aniline **3** in a multistep approach similar similar to that used for **1a**−**e**. Two precursors for diazo coupling reactions, **6** and **7**, were prepared by a two-step approach involving reductive amination[10] and hydrolysis

(4) (a) Walba, D. M.; Ros, M. B.; Clark, N. A.; Shao, R.; Robinson, M. G.; Liu, J. Y.; Johnson, K. M.; Doroski, D. J. *J. Am. Chem. Soc.* **1991**, *113*, 5472. (b) Trollsås, M.; Orrenius, C.; Sahlén, F.; Gedde, U. W.; Norin, T.; Hult, A.; Hermann, D.; Rudquist, P.; Komitov, L.; Lagerwall, S. T.; Lindström, J. *J. Am. Chem. Soc.* **1996**, *118*, 8542. (c) Dubois, J.-C.; Barny, P. L.; Mauzac, M.; Noel, C. In *Handbook of Liquid Crystals*; Demus, D., Goodby, J. W., Gray, G. W., Spiess, H. W., Vill, V., Eds.; Wiley-VCH: Weinheim, Germany, 1998; Vol. 3, p 207. (d) Artal, C.; Ros, M. B.; Serrano, J. L.; Pereda, N.; Etxebarria, J.; Folcia, C. L.; Ortega, J. *Macromolecules* **2001**, *34*, 4244. (e) Keller, P.; Shao, R.; Walba, D. M.; Brunet, M. *Liq. Cryst.* **1995**, *18*, 915. (f) Walba, D. M.; Keller, P.; Shao, R.; Clark, N. A.; Hillmyer, M.; Grubbs, R. H. *J. Am. Chem. Soc.* **1996**, *118*, 2740. (g) Fazio, V. S. U.; Lagerwall, S. T.; Zauls, V.; Schrader, S.; Busson, P.; Hult, A.; Motschmann, H. *Eur. Phys. J. E* **2000**, *3*, 245. (h) Kapitza, H.; Zentel, R.; Twieg, R. J.; Nguyen, C.; Vallerien, S. U.; Kremer, L. F.; Wilson, C. G. *Adv. Mater.* **1990**, *2*, 539. (i) Espinet, P.; Etxebarria, J.; Folcia, C. L.; Ortega, J.; Ros, M. B.; Serrano, J. L. *Adv. Mater.* **1996**, *8*, 745.
(5) (a) Ikeda, T.; Sasaki, T.; Ichimura, K. *Nature* **1993**, *361*, 428. (b) Sasaki, T.; Ikeda, T.; Ichimura, K. *J. Am. Chem. Soc.* **1994**, *116*, 625.
(6) (a) Walba, D. M.; Dyer, D. J.; Sierra, T.; Cobben, P. L.; Shao, R.; Clark, N. A. *J. Am. Chem. Soc.* **1996**, *118*, 1211. (b) Walba, D. M.; Xiao, L.; Keller, P.; Shao, R.; Link, D.; Clark, N. A. *Pure Appl. Chem.* **1999**, *71*, 2117. (c) Walba, D. M.; Xiao, L.; Korblova, E.; Keller, P.; Shoemaker, R.; Nakata, M.; Shao, R.; Link, D. R.; Coleman, D. A.; Clark, N. A. *Ferroelectrics* **2004**, *309*, 77.
(7) Wu, X.; Wu, J.; Liu, Y.; Jen, A. K.-Y. *J. Am. Chem. Soc.* **1999**, *121*, 472.
(8) Haghbeen, K.; Tan, E. W. *J. Org. Chem.* **1998**, *63*, 4503. Note that 14 g of K_2CO_3 should be used instead of 1.4 g mentioned in the experimental procedure of this reference.
(9) Bell, K. H. *Tetrahedron Lett.* **1986**, 2263.
(10) Abdel-Magid, A. F.; Carson, K. G.; Harris, B. D.; Maryanoff, C. A.; Shah, R. D. *J. Org. Chem.* **1996**, *61*, 3849.

Table 1. Mesophases, Phase Transition Temperatures, Maximum Absorption Wavelengths (λ_{max}), and the Corresponding Molar Extinction Coefficients (ε) of Compounds **1a**−**e** and **2a**−**c**[a]

compd	*T*/°C	λ_{max}/nm	ε/M^{-1} cm^{-1}
1a	Cr 65 SmC* 180 SmA* 218 Iso Iso 214 SmA* 179 SmC* 40 gSmC*	385	10757
1b	Cr 56 SmC* 136 SmA* 170 Iso Iso 160 SmA* 127 SmC* 33 gSmC*	385	9916
1c	Cr 74 SmC* 157 SmA* 174 Iso Iso 170 SmA* 155 SmC*8 gSmC*	385	9409
1d	Cr_1 60 Cr_2 98 SmC* 180 SmA* 199 Iso Iso 195 SmA* 178 SmC* 14 gSmC*	385	10812
1e	Cr 74 SmC* 168 SmA* 214 Iso Iso 204 SmA* 159 SmC* 43 gSmC*	385	10295
2a	Cr 73 Iso Iso 68 SmC* 10 gSmC*	531	30081
2b	Cr 69 Iso Iso 67 SmC* 1 gSmC*	531	29098
2c	Cr 73 SmC* 78 Iso Iso 73 SmC* 14 gSmC*	531	33912

[a] Phase transition temperatures determined by DSC at 10 K min^{-1} during heating (top) and cooling (bottom) scans from −10 (or 200) to 200 (or −10) °C, except for **1a** and **1e** from −10 (or 220) to 220 (or −10) °C. Abbreviations: Iso, the isotropic liquid; gSmC*, the glassy state of the SmC* phase; Cr, the crystalline state. The isotropic melt was stored in vials at room temperature for some time (1 week for **1a**−**e** and 3 months for **2a**−**c**) prior to DSC measurements. UV−vis spectra were taken in dilute CH_2Cl_2 solution.

under basic conditions (for **6**) and a literature[6a] approach (for **7**). Diazo coupling between them furnished diphenol **8**, which was further esterified with various 4′-alkoxy-4-biphenylcarboxylic acid chlorides to afford **2a**−**c** in good yields. It is notable that the phenol group *ortho* to the nitro group showed much higher reactivity than the one *ortho* to the diazo unit, making it possible to efficiently synthesize compounds (e.g., **2c**[11]) having different alkoxy tails attached to their biphenyl cores. All compounds were purified by flash columnar chromatography, and for some compounds, further purification was performed by crystallization from a mixture of hexanes and ethyl acetate. Analytic data are in good agreement with the proposed structures. The liquid crystalline phases were characterized by polarized-light optical microscopy (POM), differential scanning calorimetry (DSC), X-ray diffraction (XRD) analysis, and electro-optical techniques.

LC Phases of Compounds 1a−e Incorporating an Azobenzene Chromophore. Phase transition temperatures and UV−vis spectroscopic data for **1a**−**e** and **2a**−**c** are summarized in Table 1. Compounds **1a**−**e** exhibit a phase sequence of *Cr-SmC*-SmA*-Iso*. They show moderate enantiotropic SmA* phase ranges from 17 to 46 K and extremely broad enantiotropic SmC* phase ranges from 80 to 115 K during heating. Compound **1a**, with saturated alkoxy tails, shows the highest clearing point of 218 °C, and incorporation of multiple double bonds (e.g., linolyl group in **1b**)[12] and large carbosilane units (e.g., dicarbosilane unit in **1c**) into alkoxy tails significantly lowers the clearing points by 44−48 °C.

The SmC* phases of **1a**−**e** are supercooled to the glassy state, which is supported by the DSC measurements of samples after prolonged storage at room temperature. For instance, during the first heating of DSC measurements with two consecutive scans,

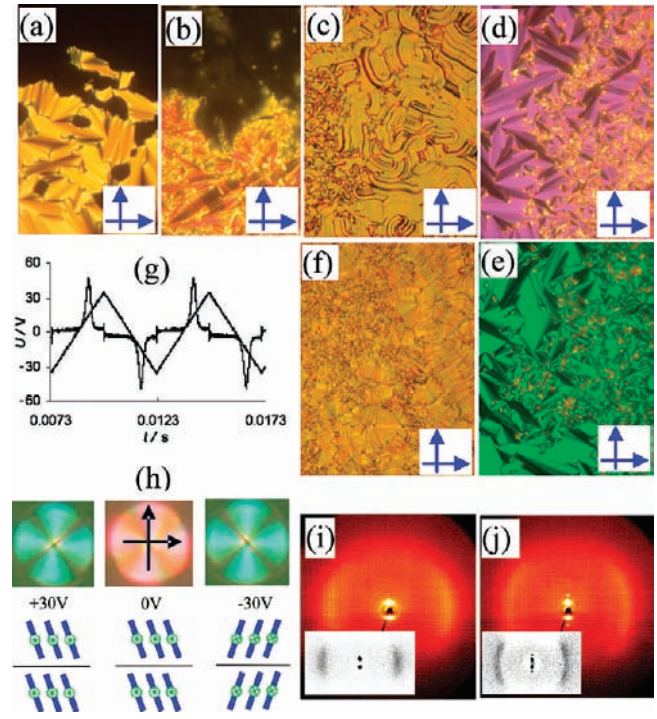

Figure 1. Textures (a, b, c, d, e, f, h) in a 6 μm ITO-coated cell, switching current response curve (g), and XRD patterns (i, j) [insets: $I = I(T) - I(177$ °C), where the scattering of the isotropic liquid is subtracted to enhance the effect of the outer diffuse scattering] of **1c**: (a, i) SmA* phase at 160 °C; (b, c, d, e, f, h, j) SmC* phase; (b) 150 °C; (c) 150 °C with field off; (d) 150 °C upon applying a square wave (SW) voltage (±30 V, 100 Hz); (e) 60 °C upon applying a SW voltage (±30 V, 20 Hz); (f) 60 °C with field-off; (g) switching current recorded in a 6 μm ITO-coated cell at 100 °C; (h) circular domains (upper, 100 °C) surrounded by void and associated director orientation (lower); (j) 140 °C.

a large endothermic peak (two peaks for **1d**),[13] attributed to a transition from the crystalline state to the SmC* phase, was observed, while this peak was not observed during the second heating, supporting a slow crystallization process. We also observed the occurrence of crystallization from the supercooled glassy state of the SmC* phase in cells during storage at room temperature and found that the speed of crystallization depends on the structure of the tails. Compounds **1c** and **1d**, with silane termini, tend to crystallize more slowly than other analogues.

Cooling the isotropic liquid of **1c** with field off yielded coexisting planar (fan-shaped texture) and homeotropic (pseudo-isotropic texture) regions (Figure 1a), suggesting a SmA* phase. Upon cooling further, the homeotropic area evolved into a *Schlieren* texture, and in the planar area an equidistant line pattern (Figure 1b) due to the helical superstructure appeared on the fan-shaped texture.[14] They are typical features for SmC* phases. We found that the optical retardation of cells filled with **1a**−**e** is strongly dependent on electric fields and temperature. For example, if no electric field was applied, **1c** exhibited various yellowish textures (Figure 1c,f) depending on temperature. Upon the application of an external electric field, green-blue fan-shaped textures (Figure 1e) were observed over the broad temperature range of the SmC* phase. As the temperature

(11) The synthesis of **2c** involved sequential addition of 4′-decyloxy-4-biphenylcarboxylic acid chloride and 4′-(11-undecenyloxy)-4-biphenylcarboxylic acid chloride, respectively by utilizing the regioselectivity due to the nitro group.

(12) Dyer, D. J.; Walba, D. M. *Chem. Mater.* **1994**, *6*, 1096.

(13) The first peak in **1d** was attributed to a transition from the first crystalline state to the second crystalline state, and the second peak was assigned as a transition from the second crystalline state to the SmC* phase. See DSC data in Table 1.

(14) Dierking, I. *Textures of Liquid Crystals*; Wiley-VCH: Weinheim, Germany, 2003.

approached the SmC*-SmA* phase transition during heating, green-blue fan textures suddenly changed to violet fan-shaped textures (Figure 1d) and eventually to yellowish fan-shaped textures (Figure 1a) in the SmA* phase. This is presumably due to the changes of birefringence and molecular tilt upon approaching the C-A transition.

Switching experiments are important for the identification of ferroelectric (FE) and antiferroelectric (AF) switching in polar mesophases. We have investigated the switching behavior of **1a**, **1c**, and **1d** by applying a triangular wave (TW) voltage. All of them show a sharp single-current peak during each half period of the TW voltage (Figure 1g), indicating FE switching. Spontaneous polarizations (*Ps*) were measured to be 112 (**1a**), 86 (**1c**), and 103 nC cm^{-2} (**1d**), respectively. The polarizations do not vary significantly except as the temperature approaches the SmC*-SmA* phase transition, indicating that the tilt angles and order parameters do not change significantly over the broad SmC* phase ranges. Cooling the isotropic liquid of **1c** under a TW voltage yielded circular domains with extinction crosses inclined with respect to crossed polarizers (Figure 1h). Reversing a DC electric field resulted in the rotation of extinction crosses, and they remained unchanged upon switching off the field. This bistable switching via rotation of molecules on a smectic cone clearly indicates a FE ground state, which confirms the result of the switching current response under the applied TW voltage.

2D XRD patterns of **1c** (Figure 1i,j) confirm the aforementioned phase sequence with layer spacings of $d_A = 3.91$ nm and $d_C = 3.84$ nm.[15] The outer diffuse scattering (ODS) in the wide-angle region shows one maximum at 0.51 nm for the SmA* phase and at 0.50 nm for the SmC* phase, which is related to the average width of the aromatic cores and the fluid alkyl chains. The tilt angle was calculated as 26° from the χ-distribution of the ODS (Figures S1 and S2), close to the optical tilt angle of 22°.[16]

LC Phase of Compounds 2a−c Incorporating a DR-1 Chromophore. Compound **2c** exhibits an enantiotropic SmC* phase with a wide range of 59 K during cooling, whereas **2a**,**b** exhibit a monotropic SmC* phase. Like for analogues **1a**−**e**, their SmC* phase is supercooled to the glassy state. In the DSC cooling scans only one exothermic peak, attributed to a transition from the isotropic liquid to the SmC* phase, was observed beside a broad glass transition step between 1 and 14 °C. Since the supercooled glassy state is metastable, crystallization can occur slowly during storage at room temperature (days to weeks).[17] As expected, crystallization of **2c** with a combination of different tails from the supercooled glassy state of the SmC* phase is slowest. Compound **2c** possesses the highest clearing point, suggesting that mixed alkoxy tails in this type of mesogenic materials stabilize the SmC* phase.

(15) The calculated molecular length for **1c** from the MOPAC molecular modeling is 4.4 nm on the basis of the rod with the azo group *meta* to the chiral center.

(16) The optical tilt angle was measured at 140 °C in an aligned 1.2 μm cell with nylon alignment layers upon the application of a SW voltage (±10 V, 10 Hz) and kept almost a constant value of 22° when the temperature was decreased from 140 to 100 °C.

(17) Crystallization was observed when cells were stored at room temperature for several days (e.g., **2a**) or several weeks (e.g., **2c**). In addition, a large endothermic peak due to a transition from the crystalline state to the SmC* phase was observed during the first heating cycle of a DSC scan when the samples were stored at room temperature for months, but the same peak could not be observed if the samples were stored at room temperature for a short time. These observations strongly indicate that crystallization from the glassy state takes place slowly during storage of samples.

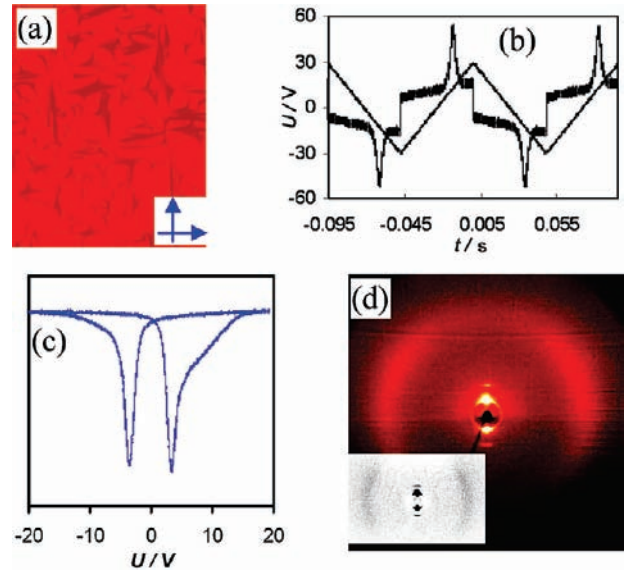

Figure 2. (a) Texture at 70 °C in a 6 μm ITO-coated cell, (b) switching current response curve at 70 °C in a 1.8 μm ITO-coated cell with parallel nylon alignment layer, (c) optical response at 65 °C in a 1.2 μm ITO-coated cell with parallel nylon alignment layer, and (d) XRD pattern at 60 °C [inset: $I = I(60\ °C) - I(80\ °C)$] of **2c**.

Cooling **2c** from the isotropic liquid yielded fan-shaped focal conic textures (Figure 2a), supporting the SmC* phase. The switching current curve shows only one single current peak (Figure 2b) during each half-period of an applied TW voltage, suggesting FE switching. Spontaneous polarizations were measured to be 65 (**2a**), 62 (**2b**), and 70 nC cm^{-2} (**2c**), respectively, which are consistent with the extrapolated polarization (65 nC cm^{-2}) reported for a dimethylamino analogue.[6a] Upon the application of a square wave (SW) field (25 V/μm), the switching time constants of **2c** were measured to be 3 ms at 70 °C and 0.5 s at 30 °C, thousands of times slower than those for conventional rod-shaped FLCs,[18] indicating high viscosity for this type of material. The FE switching was stopped by freezing a cell with dry ice but started again upon warming it up to room temperature, strongly supporting the DSC result that the SmC* phase is supercooled to the glassy state. The electro-optical response (Figure 2c) of **2c** in an aligned cell upon the application of a low-frequency (1 Hz) TW voltage shows a typical shape that does not change except for the change of the distance between two peaks as the frequency is increased (10 Hz) or decreased (0.2 Hz). These results strongly support a bistable FE switching rather than an analogous V-shaped switching.

The XRD pattern (Figure 2d) confirms the SmC* phase with a layer spacing of $d_C = 2.91$ nm and a maximum ODS at 0.45 nm. The tilt angle was calculated as 26° (Figures S1 and S3), close to the optical tilt angle of 21°[19] but much smaller than that (44°) calculated from $\cos\theta = d_C/L$,[20] suggesting strong intercalation between adjacent layers.

Textures of Racemic 1c and 2c under Homeotropic Conditions. To confirm whether the ground-state structure is synclinic FE (SmC*) or anticlinic AF (SmC_A*) in these two

(18) Conventional rod-shaped FLCs' switching speed is 10−150 μs.

(19) The optical tilt angle was measured at 60 °C in an aligned 1.2 μm cell with nylon alignment layers upon the application of a SW voltage (±20 V, 10 Hz).

(20) L is the sum (3.99 nm) of the molecular length (3.75 nm) from the MOPAC molecular modeling and van der Waals diameter (0.24 nm) of an H atom.

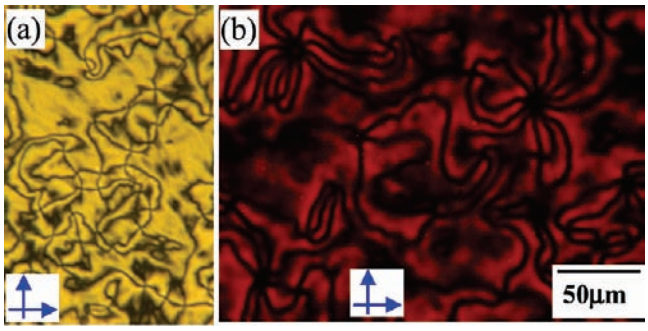

Figure 3. *Schlieren* textures of **rac-1c** (a) (normal defect strengths, $S = \pm 1$) and **rac-2c** (b) (high defect strengths, $S = \pm 1$, -2, and -3) at room temperature in a 1 μm cell under homeotropic anchoring conditions. Note that the textures at the high-temperature SmC phases are completely identical, which is additional evidence to show that the SmC* phases are supercooled to the glassy state.

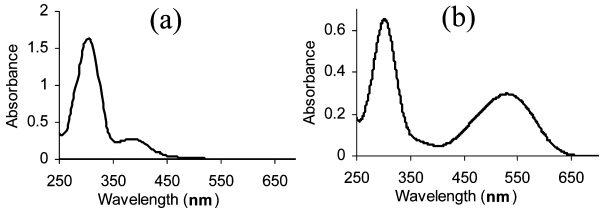

Figure 4. UV−vis spectra of **1c** (a) and **2c** (b) in dilute CH_2Cl_2 solution, showing two absorption bands.

types of H-shaped FLC materials,[21] we formulated two racemates, **rac-1c** and **rac-2c**, by mixing equimolar amounts of the corresponding enantiomers. DSCs (Figure S4) show that both exhibit almost the same phase transitions as their single enantiomers. *Schlieren* textures under homeotropic conditions[22] show only 4-brush (**rac-1c**, Figure 3a) or high-strength 4*n*-brush (**rac-2c**, Figure 3b) singularities. It was shown that SmC_A phases exhibit both 2- and 4-brush singularities while SmC phases show only 4-brush singularites.[23] This strongly supports that both **1c** and **2c** possess ground-state FE (SmC*) rather than AF (SmC_A*) phases.

UV−Vis Spectra. Both **1a**−**e** and **2a**−**c** exhibit two absorption bands in the ultraviolet and visible regions (see examples in Figure 4). The same absorption band at 304 nm is attributed to the $\pi-\pi^*$ transition of biphenyl units since the biphenol precursors **5** and **8** do not exhibit this band while 4′-decyloxy-4-biphenylcarboxylic acid chloride shows a similar band at 328 nm. The different absorption bands at 382 (**1a**−**e**) and 531 nm (**2a**−**c**) arise from the $\pi-\pi^*$ transitions of the chromophore units. Compared with **1a**−**e**, **2a**−**c** show a red-shift of 149 nm and larger molar extinction coefficients (see Table 1) for the second absorption bands, which is due to the strong charge-transfer in the DR-1 chromophore.

LC Phases of Mixtures M1 and M2. Since **2a**−**c** have a strong, broad absorption band at 531 nm (Figure 4b),[24] we have chosen to perform SHG measurements using mixtures instead of pure compounds. Compound **1c** appears to be a good SmC* host material because it is transparent at 532 nm, has a broad SmC* phase range, and forms films similar to those formed by **2c**. We formulated two mixtures, **M1** (10 mol % of **2c** in **1c**) and **M2** (20 mol % of **2c** in **1c**), and their mesophases and phase transition temperatures are listed in Table 2. As expected, mixtures **M1** and **M2** exhibit the same phase sequence as the host **1c**, but the phase transition temperatures are slightly lower than those in **1c**. As in the host **1c**, the SmC* phases in **M1** and **M2** are also supercooled to the glassy state. Crystallization slowly took place when samples were stored at room temperature for months. The bistable FE switching was confirmed by electro-optical investigations (Figure S5) similarly to those performed for the host **1c**.

Table 2. Mesophases and Phase Transition Temperatures of Mixtures[a]

mixture	*T*/°C
M1	Cr_1 55 Cr_2 71 SmC* 156 SmA* 173 Iso
	Iso 169 SmA* 154 SmC* 5 gSmC*
M2	Cr 69 SmC* 147 SmA*168 Iso
	Iso 161 SmA* 145 SmC* 5 gSmC*

[a] Phase transition temperatures determined by DSC at 10 K min^{-1} during heating (top row) and cooling (bottom row) scans from −10 (or 200) to 200 (or −10) °C. Abbreviations: Iso, the isotropic liquid; gSmC*, the glassy state of SmC* phases; Cr, the crystalline state. The isotropic melt was stored in vials at room temperature for seven months prior to DSC measurements because only the glassy transition was observed in the first heating cycle of DSC scans if the samples were stored for a short time.

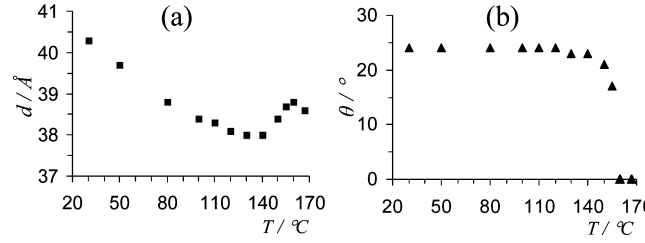

Figure 5. Plots of X-ray layer spacings (d/Å) (a) and X-ray tilt angles (θ/°) (b) of mixture **M1** versus temperature from 30 to 170 °C.

2D XRD patterns of mixture **M1** from 167 to 30 °C (Figure S6) confirm the DSC phase sequence of *Iso-SmA*-SmC*-g* during cooling. Layer spacings initially decrease from an average of $d_A = 3.87$ nm to $d_C = 3.80$ nm at 130 °C and then gradually increase to $d_C = 4.03$ nm at 30 °C (Figure 5a), whereas the X-ray tilt angles calculated from the χ-distribution of the ODS keep an almost constant value of 24° (Figure 5b) during the SmC* phase when the temperature is away from the A−C transition. This result indicates that there is strong intercalation in the SmA* phase, but the intercalation gradually weakens as the temperature is lowered during the SmC* phase (Figure 6). The increase of layer spacings without changing tilt could also be explained by a gradual C-chain stretching with decreasing temperature[25] or the combination of two effects. ODS in the wide angle region slowly increases from 0.46 nm at 30 °C to 0.50 nm at 167 °C, indicating that thermal fluctuation gradually increases the average lateral distances between the molecules.

SHG Measurements. In order to measure d_{ij} coefficients via SHG, we fabricated cells (see details in Figure S7) with

(21) Sometimes a ground-state SmC_A* material can also exhibit one current peak per half cycle owing to the merging of two current peaks. See the merge with increasing frequencies in a SmC_A* phase in ref 14, p 124.
(22) Cell surfaces were treated with *n*-octadecyltriethoxysilane to form self-assembled monolayers to achieve homeotropic alignment.
(23) (a) Takanishi, Y.; Takezoe, H.; Fukuda, A.; Komuara, H.; Watanabe, J. *J. Mater. Chem.* **1992**, *2*, 71. (b) Nishiyama, I.; Yamamoto, J.; Goodby, J. W.; Yokoyama, H. *J. Mater. Chem.* **2003**, *13*, 2429.
(24) The SHG signal at 532 nm generated from the incident beam (λ = 1064 nm) is almost entirely absorbed by **2a**−**c**. Absorption can be significantly reduced by using a small percentage of **2a**−**c**.
(25) The C-chains might be strongly folded at high temperature due to the special H-shape of the molecules and gradually stretch with decreasing temperature.

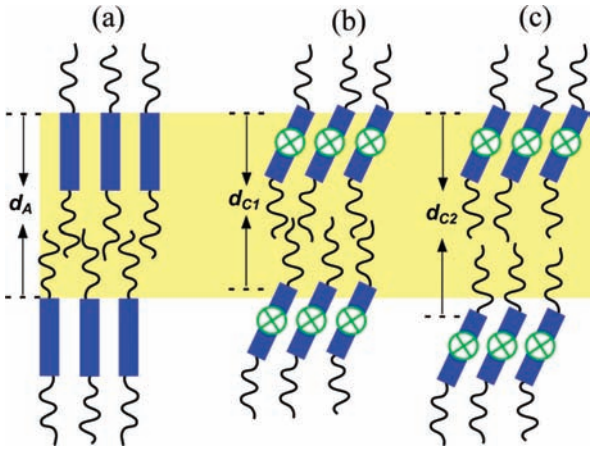

Figure 6. Models showing the organization of molecules of **M1** (a) in the SmA* phase with strong intercalation of alkoxy tails (d_A), (b) in the SmC* phase with gradually reduced intercalation of alkoxy tails (d_{C1}), and (c) in the SmC* phase without intercalation of alkoxy tails (d_{C2}). The molecules in (a−c) are viewed along the direction with the chromophore plane perpendicular to the paper. It can be conceived that the host **1c** might have the same molecular organization.

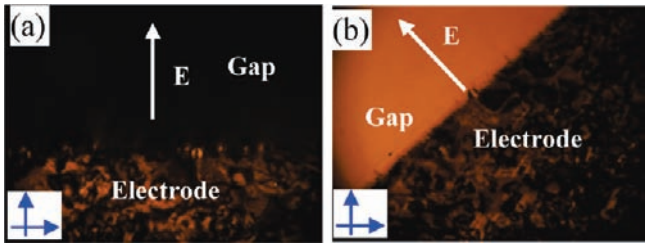

Figure 7. Textures of one of the aligned samples of mixture **M1** used for SHG measurements (1 μm thickness, 120 °C, DC voltage of 300 V across the gap of 1.7 mm). (a) Polarizers along the indicatrix axes and (b) the cell rotated by ∼45°, showing a uniform single domain in the gap. Owing to the large width of the gap, only one of the electrode edges is observed in the pictures. The electric field direction (E) is sketched in both pictures. The width of the pictures is 1 mm.

homeotropic alignment layers in the gap between in-plane ITO electrodes. Mixtures were introduced into the cells by capillary action at a temperature well above their clearing points. Samples were well oriented in these homeotropic cells (see an example in Figure 7) by applying an external strong DC electric field. The SHG experimental setup has been described elsewhere.[26] The fundamental light source is a *Q*-switched Nd:YAG (yttrium aluminum garnet) laser (λ = 1064 nm). A *y*-cut quartz crystal (d_{11} = 0.4 pm/V) was used for calibration.

The measurements were carried out at normal incidence. As shown in Figure 8, the **d** tensor is expressed in a reference frame in which *z* is perpendicular to the smectic layers and *y* is parallel to the polar axis. Input−output light polarization configurations, i.e., input and output parallel or perpendicular to the applied electric field, *p* or *s*, were used to measure SHG.

The temperature dependence of the SHG signal for mixture **M1** (Figure 9a) was investigated to find the optimum temperature for SHG efficiency. Upon cooling the isotropic liquid under a DC voltage of 400 V, a weak SHG signal was detected at 170 °C. The signal gradually increased with decreasing temperature and finally reached a maximum at 50 °C. Further cooling to 30 °C hardly affected the signal intensity. Upon

(26) Pereda, N.; Folcia, C. L.; Etxebarria, J.; Ortega, J.; Ros, M. B. *Liq. Cryst.* **1998**, *24*, 451.

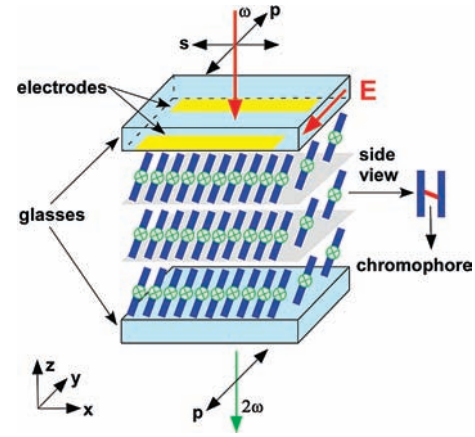

Figure 8. Scheme of the geometry of FLC molecules of mixture **M1** in the aligned zone and polarization of the input and output beams used in SHG experiments: *p*−*p* and *s*−*p*. Note that the definition of dipole herein is from positive to negative charges, as used in chemistry. The angles between the chromophore and the polar axis are about 26−30°.

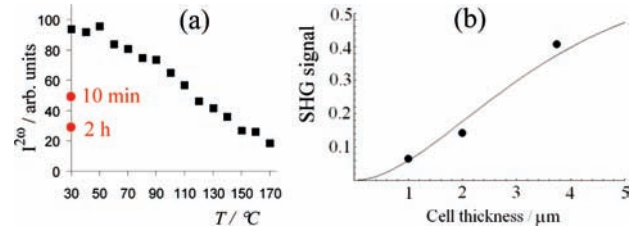

Figure 9. Temperature dependence of the SHG signal (a) in a 3.75 μm thick cell with a gap of 0.65 mm between in-plane electrodes under a DC voltage of 400 V, and SHG signal intensity normalized to the maximum signal of a quartz sample versus cell thickness (μm) (b) for mixture **M1**. All data in (b) are corrected for the *Fresnel* factors.

switching off the electric field at 30 °C, the signal dropped to half after 10 min and to the same level as that at 150 °C after 2 h. The slow dropping of the SHG signal may suggest that the supercooled SmC* phase slowly relaxes to the ground-state helical superstructure, as observed in Figure 1b.

To determine d_{ij} coefficients, we measured the SHG signal intensities of **M1** in three well-aligned homeotropic cells with thicknesses of 1.0, 2.0, and 3.75 μm. These data were compared with the SHG at the maximum of the first Maker fringe of a quartz sample (d_{11} = 0.4 pm/V) under the same conditions of illumination. Similarly, the SHG of mixture **M2** was also measured in two cells with thicknesses of 1.0 and 3.75 μm. The data process to extract the *d* coefficients followed the same approach proposed by Herman and Hayden for absorbing materials.[27]

SHG Data Process. Assuming that absorption occurs only at 2ω and the normal incidence is adopted, the SHG power $P_{2\omega}$ from an absorbing material can be simplified to

$$P_{2\omega} \propto P_{\omega}^2 d_{\text{eff}}^2 L^2 \, e^{-(\alpha_2 L/2)} \frac{\sin^2\left(\frac{2\pi\Delta nL}{\lambda}\right) + \sinh^2\left(\frac{\alpha_2 L}{4}\right)}{\left(\frac{2\pi\Delta nL}{\lambda}\right)^2 + \left(\frac{\alpha_2 L}{4}\right)^2}$$

where $d_{\text{eff}} = d_{22}$ for *p*−*p* polarizations, α_2 is the absorption coefficient at 2ω, and its value (0.614 μm^{-1}) for mixture **M1** is extrapolated from the UV−vis spectrum of **2c** in dilute CH_2Cl_2 solution, $\Delta n = n_o(2\omega) - n_o(\omega)$ is the corresponding ordinary

(27) Herman, W. N.; Hayden, L. M. *J. Opt. Soc. Am. B* **1995**, *12*, 416.

refractive index mismatch between the second harmonic and fundamental waves, λ is the wavelength of the fundamental light, L is the sample thickness, and P_ω is the power of the fundamental light. A fit of SHG intensities (normalized to quartz) of the three samples of **M1** to a theoretical curve (Figure 9b) gives the d_{22} coefficient (1.5 pm/V) and the dispersion parameter $\Delta n = 0.01$. The same treatment for **M2** produces the d_{22} coefficient (3.9 pm/V) and the dispersion parameter $\Delta n = 0.02$. This is the first use of SHG to characterize absorbing NLO FLC materials. The remaining d_{ij} coefficients can be deduced from the other polarization configuration and were much smaller than d_{22}. The SHG measurement of the host **1c** is negligible in comparison with **M1** and **M2**. Hence, using a linear extrapolation formula, the d_{22} coefficient of **2c** was found to be 17 pm/V,[28,29] more than 3 times as large as that for the best calamitic NLO FLC previously reported, Roche-1.[30,31] This d value is also larger than those reported for most bent-core compounds.[32] The electro-optical (EO) coefficient r_{22} is estimated to be larger than 5 pm/V,[33] which is comparable to the r coefficients of many commercial inorganic EO crystals.

Conclusion

We report two new classes of laterally azo-bridged FLCs that incorporate azobenzene and DR-1 chromophores along the FLC polar axes. Compounds **1a**−**e**, containing an azobenzene chromophore, exhibit thermodynamically stable enantiotropic SmA* and SmC* phases, while **2c**, incorporating a DR-1 chromophore, only has an enantiotropic SmC* phase. They are the first H-shaped dimesogens that have ground-state enantiotropic FE phases. Both mixtures **M1** and **M2** also exhibit ground-state FE phases. It is remarkable that they can readily achieve good planar alignment in cells with buffed nylon alignment layers and good homeotropic alignment under a relatively weak in-plane electric field.

SHG measurements of mixtures give the extrapolated d_{22} coefficient of 17 pm/V, the largest NLO coefficient reported to date for calamitic FLCs. This value enables viable applications of FLCs in nonlinear optics. To the best of our knowledge, this work represents the first example that combines intrinsic polar order with large macroscopic nonlinearities. It should be noted that, although some bent-core NLO mesogens show large macroscopic nonlinearities, almost all of them have ground-state antiferroelectricity. These investigations indicate that elaborate molecular design and tailoring can lead to interesting stimuli-responsive functional FLC materials with potentially useful NLO and EO properties.

Acknowledgment. This work was supported by NSF (USA) grants (OII-0539835 and IIP-0646460) to Displaytech Inc., and by the CIDYT-FEDER of Spain-EU (Project MAT2006-13571-C02-02). J.M.-P. thanks the Basque Government for a grant.

Supporting Information Available: Synthetic procedures for **1a**−**e** and **2a**−**c**; cell fabrication; Figures S1−S7; and Table S1. The material is available free of charge via the Internet at http://pubs.acs.org.

JA9069166

(28) Dalton et al. have shown that dipole−dipole interaction significantly increases with increased chromophore loading for strong chromophores, but the electro-optical coefficients for polymeric materials, including DR-1 chromophores, are almost linear with chromophore loading if the chromophore density is less than 25 wt %: Dalton, L. R.; Steier, W. H.; Robinson, B. H.; Zhang, C.; Ren, A.; Garner, S.; Chen, A.; Londergan, T.; Irwin, L.; Carlson, B.; Fifield, L.; Phelan, G.; Kincaid, C.; Amend, J.; Jen, A. *J. Mater. Chem.* **1999**, *9*, 1905–1920. The DR-1 chromophore density in **2c** is 23 wt %. Moreover, we have found that **1c** and **2c** have similar degrees of polar order (∼20%) (see details in Table S1). Hence, extrapolating the d_{22} coefficient of **2c** from mixtures **M1** and **M2** is valid.

(29) Preliminary SHG measurements of pure films of **2c** at the incident wavelength of 1600 nm (much further from resonance) give an expected smaller d_{22} value of 4.5 pm/V, which is still remarkable for calamitic FLCs. This result, together with SHG measurements of mixtures **M1** and **M2** at the same wavelength, will be published separately.

(30) Schmitt, K.; Herr, R. P.; Schadt, M.; Fünfschilling, J.; Buchecker, R.; Chen, X. H.; Benecke, C. *Liq. Cryst.* **1993**, *14*, 1735.

(31) It is evident that the d value in Roche-1 including a *p*-nitroaniline chromophore is less resonantly enhanced than that in **2c** containing a DR-1 chromophore. However, the β value of DR-1 is more than 5 times that of *p*-nitroaniline at the incident wavelength of 1.91 μm (49 vs 9.2×10^{-30} esu): Cheng, L. T.; Tam, W.; Stevenson, S. H.; Meredith, G. R.; Rikken, G.; Marder, S. R. *J. Phys. Chem.* **1991**, *95*, 10631–10643. Their dispersion-free values β_0 (35.2 vs 7.6×10^{-30} esu) are extrapolated using the two-level model: Spackman, M. A. *J. Phys. Chem.* **1989**, *93*, 7594. Furthermore, the degree of polar order for Roche-1 (∼30%, see ref 6a) is only 50% larger than that (∼20%, see Table S1) for **2c**. Taking these factors into account, a large d_{22} value (17 pm/V) for **2c** is reasonable.

(32) (a) Ortega, J.; Gallastegui, J. A.; Folcia, C. L.; Etxebarria, J.; Gimeno, N.; Ros, M. B. *Liq. Cryst.* **2004**, *31*, 579. (b) Araoka, F.; Thisayukta, J.; Ishikawa, K.; Watanabe, J.; Takezoe, H. *Phys. Rev. E* **2002**, *66*, 021705. (c) Folcia, C. L.; Alonso, I.; Ortega, J.; Etxebarria, J.; Pintre, I.; Ros, M. B. *Chem. Mater.* **2006**, *18*, 4617. (d) Etxebarria, J.; Ros, M. B. *J. Mater. Chem.* **2008**, *18*, 2919–2916. Note that big differences for d coefficients of similar bent-core compounds were reported by different groups, and the reasons are still unclear.

(33) The analogue with an opposite DR-1 chromophore dipole orientation was reported to give an extrapolated coefficient of $r \approx 5$ pm/V: Walba, D. M.; Garcia, E.; Niessink-Trotter, J.; Richard, M.; Shao, R.; Nakata, M.; Clark, N. A. Presented at the 22nd International Liquid Crystal Conference, ILCC 2008, June 29−July 4, 2008, Jeju, Korea; Abstracts I, p 228. Moreover, we found that its homologue with a diethylamino donor shows a blue shift of >60 nm for the maximum absorption wavelength in comparison to **2c**, suggesting a smaller β value for the analogue than that for **2c**. Taking into account these factors, we can deduce that the practical r_{22} value for **2c** should be larger than 5 pm/V.